Science Bulletin 64 (2019) 547–552

Contents lists available at ScienceDirect

Science Bulletin

journal homepage: www.elsevier.com/locate/scib

Science Bulletin
www.scibull.com

Article

Chlorine capped SnO_2 quantum-dots modified TiO_2 electron selective layer to enhance the performance of planar perovskite solar cells

Tingting Wu [a,b,1], Chao Zhen [a,1], Jinbo Wu [a,b], Chunxu Jia [a,b], Mustafa Haider [a,c], Lianzhou Wang [d], Gang Liu [a,b,*], Hui-Ming Cheng [a,e]

[a] Shenyang National Laboratory for Materials Science, Institute of Metal Research, Chinese Academy of Sciences, Shenyang 110016, China
[b] School of Materials Science and Engineering, University of Science and Technology of China, Shenyang 110016, China
[c] University of Chinese Academy of Sciences, Beijing 100049, China
[d] Nanomaterials Centre, School of Chemical Engineering and AIBN, The University of Queensland, Brisbane, QLD 4072, Australia
[e] Low-Dimensional Material and Device Laboratory, Tsinghua-Berkeley Shenzhen Institute, Tsinghua University, Shenzhen 518055, China

ARTICLE INFO

Article history:
Received 5 March 2019
Received in revised form 23 March 2019
Accepted 2 April 2019
Available online 3 April 2019

Keywords:
TiO_2
SnO_2 quantum dots
Interface modification
Perovskite solar cells

ABSTRACT

SnO_2 quantum dots (QDs) ended with chlorine ions are introduced at the interface of spin-coated TiO_2 electron selective layer (ESL)/perovskite to fill the pinholes in the layer and passivate the trapping defects. As a result of the increased interface electron collection and reduced bulk recombination, the planar perovskite solar cell with the QDs modified ESL gives the large power conversion efficiency enhancement from 14.9% to 17.3% and greatly improved stability under the continuous light irradiation.

1. Introduction

Metal halide perovskite solar cells (PSCs) have attracted intensive attention due to the merits of simple solution fabrication process, low-cost and high-efficiency [1–3]. The certified efficiency has rapidly increased to >23% since the emergence of all solid-state devices in 2011 [4,5]. The high-efficiency is intrinsically originated from the outstanding optoelectronic properties, particularly the longer photo-carrier diffusion lengths than the penetration depths of incident sunlight, of metal halide perovskite materials [6]. The photo-carriers can effectively transport through the perovskite active layer, arriving at the interfaces with the electron selective layers (ESLs) and hole selective layers (HSLs). In this situation, controlling the interface structures plays an important role in promoting the collection of photo-carriers and thus the power conversion efficiency of PSCs [7–9].

Solution processed (e.g. spin-coating) dense films of TiO_2 as the most widely used ESL material have been frequently involved in PSCs [10]. However, the planar devices based on this kind of TiO_2 ESLs generally showed moderate efficiencies with low stability under irradiation and strong hysteresis behaviour because of the presence of many pinholes in the TiO_2 films and defect trapping states at the TiO_2/perovskite interface [11]. The pinholes might cause the direct contact of bottom electrode and the perovskite active layer to increase the number of recombination centers of photo-carriers. The interfacial trapping states are also deleterious by capturing the photo-carriers to increase the carrier recombination and/or cause capacitive storage. To address these limitations, surface modification of TiO_2 ESLs has been applied to facilitate the selective photo-electron collection and suppress the charge recombination at the TiO_2/perovskite interface. Organic molecules with specific function groups such as fullerene derivative have been used to modify surface of TiO_2 ESLs by chemical monolayer adsorption to passivate the interfacial trapping states for the performance enhancement and hysteresis elimination [12]. However, the pinholes cannot be fully filled by the monolayer of organic molecules and the organic materials are prone to be destroyed under the sunlight irradiation and/or heating [13]. Alternatively, some ultrathin inorganic materials with proper band positions such as amorphous TiO_2 and SnO_2 were also explored to modify the surface of the ESLs and suppress the recombination at the interface [14,15].

Inorganic colloidal quantum dots (QDs) are a class of uniform inorganic nanocrystals with their surface passivated by a

* Corresponding author.
E-mail address: gangliu@imr.ac.cn (G. Liu).
[1] These authors contributed equally to this work.

https://doi.org/10.1016/j.scib.2019.04.009
2095-9273/

monolayer of ligands or ions. The particle size of several nanometers makes QDs a good candidate to be dispersed well on the TiO_2 ESLs and fill the pinholes. Meanwhile, their surface monolayer of ligands or ions might passivate the interfacial defects. Halide ions, which can stabilize QDs, have shown their functions of reducing the inter-particle transfer resistance and suppressing the interfacial trapping states in photovoltaic devices [16,17]. Some hysteresis-free, highly efficient and stable devices have been obtained [16]. SnO_2 with high electron mobility and low density of surface states has been frequently used as the ETL component or a modifier of TiO_2 ESLs to obtain high efficiency and hysteresis-free (or weaker) PSCs [18–20]. Considering the promising advantages of SnO_2 QDs with surface covered by proper halide ions in modifying the interface of the TiO_2/perovskite, it is desirable to explore the application of SnO_2 QDs in enhancing the device performance.

Herein, SnO_2-QDs with chlorine capping ions were introduced atop the spin-coated TiO_2 ESLs with the aim of both filling the pinholes in the film and passivating defects at the TiO_2/perovskite interface with the chlorine ions. The average efficiency was muchly improved from ~14% for the pure TiO_2 based devices to over 17% for the devices with the SnO_2 QDs modified TiO_2 ESLs. Moreover, compared to the devices with pure TiO_2, the devices with SnO_2 QDs modified TiO_2 ESLs have a narrow efficiency distribution. The combination of both the photoluminescence spectra and the electrochemical impedance spectroscopy confirms the effective electron extraction and suppression of interface charge recombination at the interface.

2. Material and methods

2.1. Device fabrication

Fluorine doped tin oxide (FTO) glass pieces were washed in deionized water with different cleaning agents including ethanol, acetone and isopropanol sequentially each for 15 min under ultrasonic conditions. Then all the pieces were treated by oxygen plasma cleaner for 5 min. A precursor solution containing 15 mL ethanol, 75 μL HCl and 900 μL tetrabutyl titanate was spin-coated on FTO surface at the speed of 5,000 r min^{-1} for 30 s to produce TiO_2 layer, followed by thermal treatment at 500 °C in air for 30 min. SnO_2-QDs solution was prepared according to Ref. [21]. 1015 mg of $SnCl_2{\cdot}2H_2O$ and 338 mg of thiourea were added into 30 mL DI water under continuous stirring for over 24 h until the color of solution changed from white to yellow. The resultant SnO_2-QDs solution was spin-coated on the TiO_2 layer surface at 5000 r min^{-1} for 30 s. In order to remove the organics, the substrates were treated on the hotplate at 200 °C for 1 h.

The deposition of perovskite films. A precursor solution was prepared by mixing FAI (1 mol L^{-1}), PbI_2 (1.1 mol L^{-1}), MABr (0.2 mol L^{-1}) and $PbBr_2$ (0.22 mol L^{-1}) in anhydrous DMF: DMSO 4:1 (v:v). The 1.5 mol L^{-1} CsI solution was added into the above solution in volume ratio 5:95. The mixed solution was spin-coated on the pristine and SnO_2-QDs modified TiO_2 films at the speed of 1,000 r min^{-1} for 10 s and followed 4,000 r min^{-1} for 30 s. In the second step, 200 μL chlorobenzene was dropped to remove the organic solvent at 20 s before the end of the first step. Subsequently, the substrates were put on a hotplate immediately to convert the precursor films into perovskite films. The samples were heated at 100 °C for 10 min. Hole selective layer (HSL) solution, containing 72.3 mg mL^{-1} of Spiro-OMeTAD, 28.8 μL mL^{-1} of *tert*-butylpyridine and 17.5 μL mL^{-1} of bis(trifluoromethane)sulfo nimide lithium salt (520 mg mL^{-1} in acetonitrile), was prepared and spin-coated on the top of perovskite films at the speed of 5,000 r min^{-1} for 30 s. Finally, a 70-nm-thick Au layer was deposited as the counter electrode by a thermal evaporation system at a base pressure $\sim 2 \times 10^{-4}$ Torr with a deposition rate of ~1 Å s^{-1}. The active area for all solar cells was 0.09 cm^2.

2.2. Device characterization

Surface morphology and cross-sectional images were recorded on a scanning electron microscope (FEI Nano SEM 430). Atom force microscope (AFM) images were recorded by Bruker multimode 8. Transmission electron microscope (TEM) images were taken on a FEI Tecnai G2 F30 operated at 300 kV. The conduction band edge positions of the samples were analyzed by ultraviolet photoelectron spectroscopy (Thermo ESCALAB 250Xi). UV–vis absorption spectra were recorded on a JASCO-770 spectrophotometer. Photoluminescence emission spectra (460 nm excitation) were measured at room temperature with a fluorescence spectrophotometer (Edinburgh Instruments, FLSP-920) and the time-resolved photoluminescence was acquired using the same equipment with 471.1 nm pulse laser as the light source. Solar cells with an active area of 0.09 cm^2 were measured in ambient air under the illumination of AM 1.5G simulator (Newport, 91192). All electrochemical testing including *J-V* curves, MPPT curves and EIS spectra were recorded on an EC-lab (BioLogic SP-200). Incident photon-to-current conversion efficiency (IPCE) was measured at zero bias on a QTest Station 1000AD (CROWNTECH).

3. Results and discussion

A TiO_2 compact film on fluorine doped tin oxide (FTO) glass substrate by a spin-coating technique shows many pinholes of tens of nanometers in diameter caused by the crystallization and thermal stress during the subsequent heating (Fig. 1a). The FTO layer has a rough surface owing to the large FTO crystal grains. The pinholes are mainly formed at the sharp corners of the FTO crystal grains, which may lead to the unfavorable direct contact of the FTO layer with perovskite active layers. The SnO_2-QDs were synthesized from a precursor solution containing $SnCl_2$ and thiourea according to the previous report [21]. The particle size of as-prepared SnO_2-QDs is 3–5 nm based on the high resolution TEM image (Fig. S1 online). The spin-coating of the colloidal SnO_2-QDs solution on the TiO_2 film and subsequent heating at 200 °C for 1 h produces a pinhole-free film (Fig. 1b). The exact distribution of SnO_2-QDs on the TiO_2 film surface cannot be recognized from SEM image due to the extremely small size of QDs. Atomic force microscopy (AFM) is a powerful tool to characterize fine structures of relatively flat substrate but its application in this case is limited by the large roughness of FTO layer. A reference TiO_2 film on a flat quartz substrate by the same method was prepared and also displays numerous pinholes of tens of nanometers (black points in the AFM image in Fig. 1c). After spin-coating of the colloidal SnO_2-QDs on the TiO_2 film, the black points (pinholes) disappear throughout the whole film, suggesting the formation of a dense film (Fig. 1d). The size of the nanoparticles located at the film top is a few nanometers, which is in agreement with the size of SnO_2-QDs measured from the high resolution TEM image.

The results from the combination of SEM and AFM images of two TiO_2 films respectively supported on the FTO glass and quartz substrates suggest the formation of a pinhole-free continuous dense film on the pristine TiO_2 film with the spin-coating of SnO_2-QDs. The pinholes in TiO_2 compact layers have the underlying negative influence on the photovoltaic performance of devices due to the serious carrier recombination at the interfaces caused by the direct contact between FTO with perovskite as shown schematically in Fig. 1e. Once the pinholes are fully filled by SnO_2-QDs, the carrier recombination pathways of the back flow of electrons to the

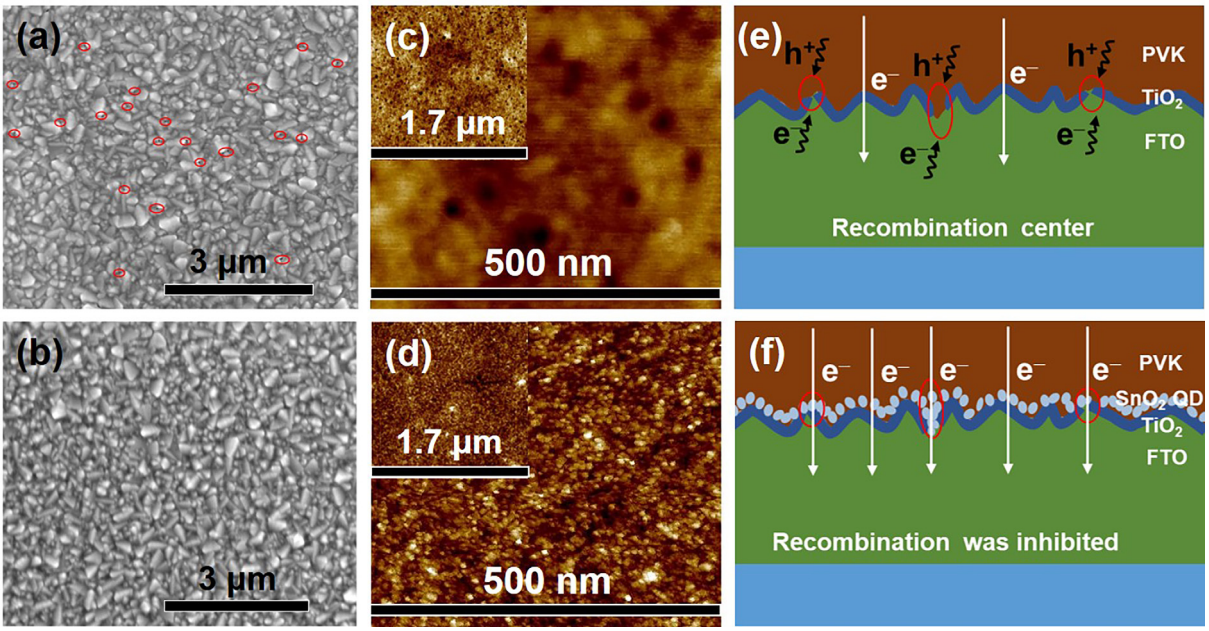

Fig. 1. (Color online) The role of SnO_2-QDs played in modifying TiO_2 layer. Top-view SEM images of (a) TiO_2 and (b) SnO_2-QDs modified TiO_2 layers on FTO glass substrates. AFM images of (c) TiO_2 and (d) SnO_2-QDs modified TiO_2 layers on quartz substrates, and the inset gives the enlarged regions in (c) and (d). Schematic of charge carrier recombination processes (e) without and (f) with SnO_2-QDs at the top of TiO_2 layer.

perovskite layer can be removed (Fig. 1f). The presence of chlorine ions as the capping agent on SnO_2-QD surface is confirmed by the strong signal of Cl^- in XPS spectrum recorded from the pristine surface of SnO_2-QD film (Fig. S2 online). The amount of Cl^- on SnO_2 surface is ~2.74 at% and the atomic ratio of Cl^- to Sn is as high as 13.6% from XPS analysis. The positive role of Cl^- at the TiO_2/perovskite interface in improving the crystallinity of perovskite and suppressing the formation of interfacial trapping-states has been validated [16]. The atomic ratio of Sn and O is close to the stoichiometric 1:2, indicating the formation of SnO_2 (Fig. S3 online).

The influence of SnO_2-QDs on the light transmittance of TiO_2 film is examined by comparing the transmittance spectra of the pristine and SnO_2-QDs modified TiO_2 films deposited on FTO glass substrates (Fig. S4 online). Little difference between their spectra in the whole visible light range suggests that the introduced thin layer of SnO_2-QDs cannot cause the optical transmittance loss. Two groups of PSCs were fabricated respectively based on the pristine and SnO_2-QDs modified TiO_2 ESLs to evaluate the effect of the SnO_2-QDs layer on the photovoltaic performance. The perovskite and HSL material used in this work were $CsMAFAPbI_xBr_{3-x}$ and 2,2′,7,7′-tetrakis(N,N-di-p-methoxyphenylamine)9,9′-spirobi-fluorene (Spiro-OMeTAD), respectively, and Au thermally deposited at the top as the counter electrode. The $CsMAFAPbI_3Br_{3-x}$ films deposited on the pristine and SnO_2-QDs modified TiO_2 ESLs were characterized by X-ray diffraction (XRD) and SEM. The formation of the $CsMAFAPbI_{3-x}Br_x$ perovskite films in the devices of both cases is confirmed by their XRD patterns (Fig. S5 online). Note that the perovskite film supported by the modified TiO_2 ESL shows sharper and stronger diffraction peaks than that deposited on the pristine TiO_2 ESL, indicating the higher crystallinity and larger crystal grains of the $CsMAFAPbI_{3-x}Br_x$ film on the former ESL. Comparison of the top-view SEM images of two films (Fig. S6 online) further confirms the bigger crystal grains for the TiO_2/SnO_2-QDs ESL case. This indicates that the SnO_2-QDs play an important role in promoting the perovskite crystal growth. Chlorine ions were proved to be effective in bridging metal halide perovskites and ESLs [16]. It is therefore proposed that the SnO_2-QDs capped with chlorine ions shall promote the growth of perovskite crystals with high crystallinity and big grains [22].

The cross-sectional SEM image of the SnO_2-QDs modified ESL based device shows a layer-by-layer structure of (FTO/ESL/$CsMAFAPbI_3Br_{3-x}$/Spiro-OMeTAD/Au) (Fig. 2a) with a high quality continuous interface between the perovskite and ESL. However, the cross-sectional SEM image of the pristine TiO_2 ETL based device shows a discontinuous interface (Fig. S7 online). This obvious difference at the perovskite/ESL interface further provides the evidence for the positive role of SnO_2-QDs in promoting perovskite growth. The thickness of perovskite layer is around 550 nm for both cases, which is thick enough for sufficient light absorption and suitable for the photo-carrier bulk separation. The absorption spectra of perovskite films on two different ESLs show nearly the same absorbance in the whole UV–vis-NIR range (Fig. S8 online).

Photovoltaic performance of PSCs based on the pristine and SnO_2-QDs modified TiO_2 ESLs was compared under the illumination of AM 1.5G sunlight simulator (power density, 100 mW cm^{-2} calibrated by a standard silicon solar cell). The champion device based on the modified ESL delivers an efficiency of 17.3% with J_{sc} of 20.7 mA cm^{-2}, V_{oc} of 1.105 V and *FF* of 75.3% (Fig. 2b). While the champion device based on the pristine ESL only shows a moderate efficiency of ~14.9% with J_{sc} of 20.48 mA cm^{-2}, V_{oc} of 1.06 V and *FF* of 68.7%. The much improved efficiency mainly results from the enlarged V_{oc} and *FF*. To further confirm this point, the current density-voltage (*J-V*) curves of two groups of the devices respectively based on the pristine and modified TiO_2 ESLs were recorded. Consistently, all devices using modified ESL give much enhanced efficiency compared to the devices based on the pristine ESL (Fig. S9 online). All the photovoltaic parameters from *J-V* curves show that the devices with the modified ESL have a much better reproducibility compared to that with the pristine ESL based devices. Moreover, the average values of V_{oc} and *FF* are significantly increased and particularly *FF* of over 75% has a very narrow distribution. The hysteresis behavior is also reduced but still exists with the modification of SnO_2-QDs (Fig. S10 online). However, the PSCs based on the modified ESL show a much improved output-power stability under the continuous light irradiation compared to the

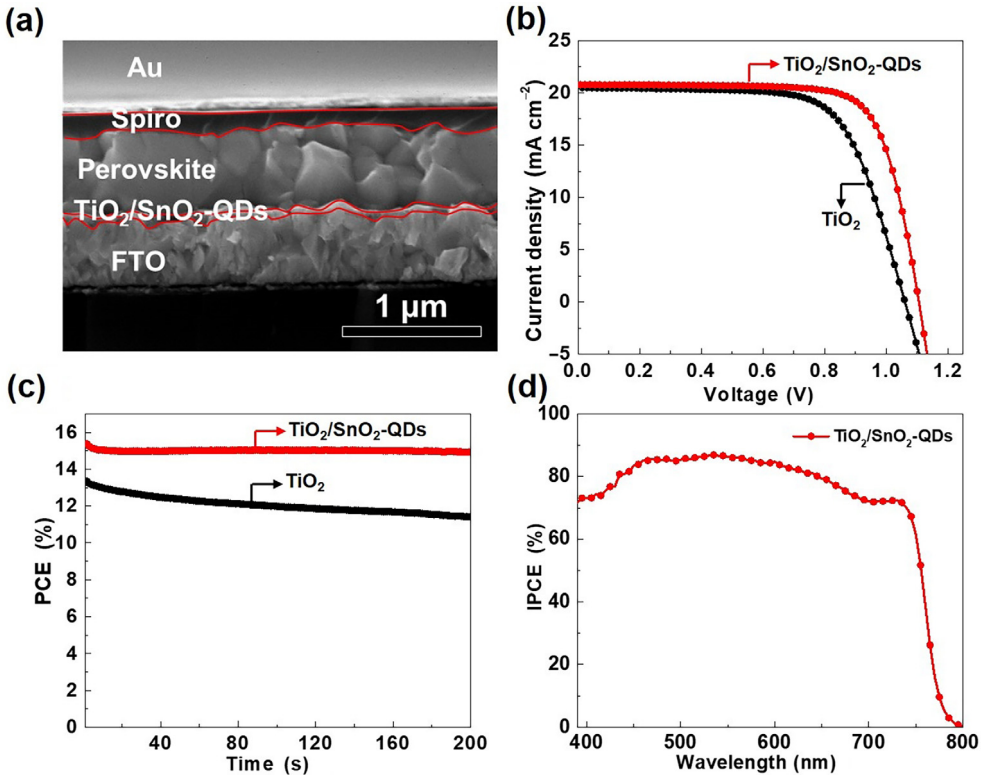

Fig. 2. (Color online) Device structure and performance. (a) Cross-sectional SEM image of a PSC based on the SnO_2-QDs modified TiO_2 ESL. (b) *J-V* curves and (c) maximum power point tracking (MPPT) recorded from two PSCs respectively based on the pristine and SnO_2-QDs modified TiO_2 ESLs. (d) IPCE curve of the champion device based on the SnO_2-QDs modified TiO_2 ESL.

devices based on the pristine ETL as confirmed by the maximum power point tracking measurements (Fig. 2c). A stable power conversion efficiency of ~15% is achieved for the device based on the modified ESL but a gradual efficiency decrease from ~13% to ~11.5% is observed for the case of unmodified ESL. The incident photon-to-current conversion efficiency (IPCE) spectrum recorded on the champion device with the modified ESL reveals that its response behavior is consistent with the absorption spectrum (Fig. 2d). Over 70% conversion efficiency in the whole visible light range and a maximum value of 87% at 535 nm are achieved. The integrated J_{sc} calculated from the IPCE spectrum is 19.6 mA cm^{-2}, which was basically in agreement with that of 20.7 mA cm^{-2} obtained from the *J-V* curve.

To understand the origin of the enhanced performance of solar cells by the introduction of SnO_2-QDs, ultraviolet photoelectron spectra (UPS) and UV–vis absorbance spectra were recorded to identify the positions of band edges of the spin-coated TiO_2 and SnO_2-QD layers. The valence band edge positions of TiO_2 and SnO_2-QDs are determined to be −7.57 and −7.93 eV versus the vacuum energy level, respectively (Fig. 3a). Considering the band gap of 3.28 eV for TiO_2 and 4.25 eV for SnO_2-QDs determined from their UV–vis absorption spectra (Fig. S11 online), the conduction band edge positions are confirmed to be –4.29 eV for TiO_2 and –3.68 eV for SnO_2-QDs. Apparently, the fact of the higher conduction band edge position of SnO_2-QDs than that of both perovskite and TiO_2 makes it unseemly beneficial for the electron transport through the conduction band. In this situation, the transport of photo-electrons might be realized easily by quantum tunneling from perovskite to the TiO_2 layer as long as the thickness of SnO_2-QD layer is thin enough. Moreover, the back flow of photo-electrons can be inhibited. The ultra-thin layer by spin-coating a low concentration of SnO_2-QDs colloid solution at a high speed can satisfy the conditions required by quantum tunneling. The photo-carrier dynamics in a PSC with the SnO_2-QDs modified ESL is illustrated schematically in Fig. 3b.

The steady photoluminescence (PL) and time-resolved PL spectra of perovskite films deposited on the pristine and modified TiO_2 ESLs were recorded to study photoelectron transfer dynamics across the perovskite/ESL interface (Fig. 4a and b). The perovskite on the modified ESL shows a much stronger PL quenching than that on the pristine ESL (Fig. 4a), indicating that the introduced SnO_2-QDs at interface facilitate the electron extraction from perovskite to ESL. Based on time resolved PL spectra (Fig. 4b), the decay times of photo-carriers are obtained by fitting with a biexponential decay equitation (Table S1 online), in which the fast decay time τ_1 and slow decay time τ_2 correspond to the photo-electron transfer across the perovskite/ESL interface and photo-carrier recombination in perovskite bulk, respectively. The fast decay lifetime τ_1 of the perovskite film on the pristine and modified ESL is 5.71 and 6.58 ns. The prolonged time τ_1 might be caused by the ultra-thin SnO_2-QDs layer at interface, which can retard the photoelectron transfer across the interface, to some extent. In contrast, the slow decay time τ_2 is largely reduced for the perovskite film on the modified ESL compared to that on the pristine ESL. The reduction of the decay time τ_2 by a factor of two times shall be associated with the high crystallinity and big crystal grains of perovskite film on the modified ESL, which facilitate the photoelectron transport towards the perovskite/ESL interface. The great reduction of the bulk recombination related time τ_2 is therefore responsible for the improved PL quenching efficiency.

The electrochemical impedance spectra (EIS) recorded on the devices based on the pristine and modified ESLs were compared to further clarify the difference in photo-carrier dynamics in the devices (Fig. S12 online). Two semicircles at the high and low frequency ranges in the Nyquist plots are related to the charge carrier transfer resistance (R_{tr}) across the interfaces and charge carrier

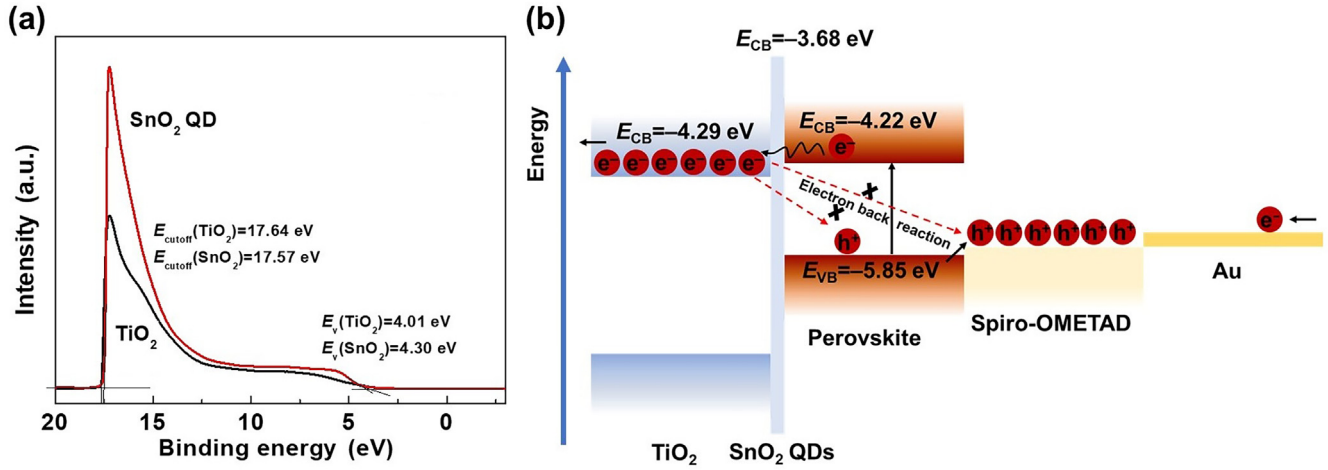

Fig. 3. (Color online) Band edge alignment and photocarrier dynamics in the resultant device. (a) Ultraviolet photoelectron spectroscopy (UPS) spectra recorded from the TiO_2 and SnO_2-QD films spin-coated on FTO glass substrates. (b) Schematic of energy level diagram of the SnO_2-QDs modified TiO_2 ESL based PSC.

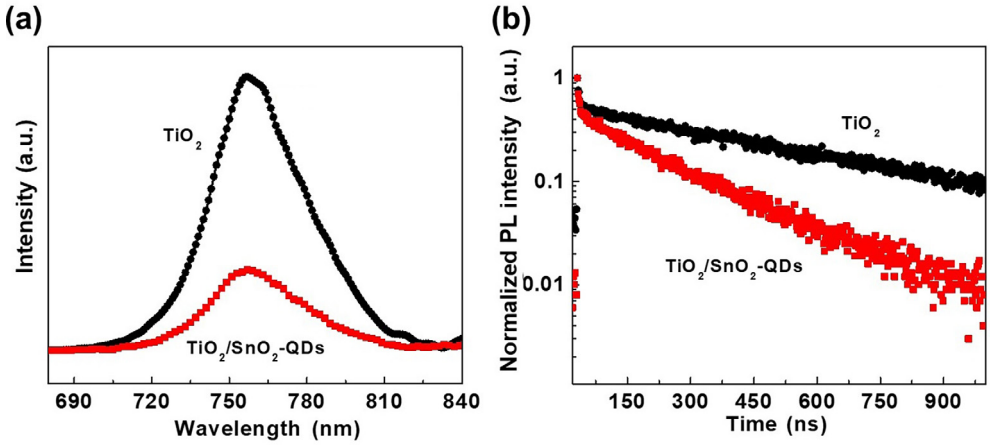

Fig. 4. (Color online) Photoelectron extraction ability analysis. (a) Steady PL and (b) time-resolved PL spectra of perovskite films on the pristine and SnO_2-QDs modified TiO_2 ESLs.

recombination resistance (R_{rec}) at interfaces. A tandem equivalent circuit (Fig. S13 online) was used to fit the Nyquist plots and the fitted interface transfer and recombination resistances are listed in Table S2 (online). A slightly increased R_{tr} for the modified ESL case is consistent with the time resolved PL result of the slightly prolonged time τ_1 as a result of the retarded photoelectron transfer across the interface. The increased R_{rec} for the modified ESL case is attributed to the filling of the pinholes in the TiO_2 film and passivation of defects at the TiO_2/perovskite interface by introducing SnO_2-QDs.

4. Conclusions

In summary, to improve photovoltaic performance of planar PSCs based on spin-coated TiO_2 ESLs, SnO_2-QDs ended with chlorine ions were used as a modifier to fill the pinholes in the spin coated TiO_2 ESL and passivate trapping defects at the TiO_2/perovskite interface. The resultant perovskite film has high crystallinity and large crystal grains as well as an improved interfacial connection with ESL because the SnO_2-QDs ended with chlorine ions can promote the nucleation and growth of the perovskite crystals. As a result of the synergy of the greatly suppressed bulk recombination in high-quality perovskite film, reduced interfacial recombination by filling the pinholes, passivated interfacial trapping defects and introduced the barrier to block back flow of the electrons, the champion efficiency is improved from 14.9% for the pristine ESL based devices to 17.3% for the modified ESL based devices. Moreover, the device with the SnO_2-QDs modified ESL gives a much more stable output-power under the continuous light irradiation.

Conflict of interest

The authors declare that they have no conflict of interest.

Acknowledgments

This work was financially supported by the National Natural Science Foundation of China (51825204) and the Key Research Program of Frontier Sciences CAS (QYZDB-SSW-JSC039).

Author contributions

GL and HMC conceived the project. TTW and CZ conducted the fabrication and measurements of the cells and wrote the manu-

script. JBW, CXJ, MH and LZW were involved in the analysis of the results. All authors revised the manuscript.

Appendix A. Supplementary data

Supplementary data to this article can be found online at https://doi.org/10.1016/j.scib.2019.04.009.

References

[1] Correa-Baena J-P, Abate A, Saliba M, et al. The rapid evolution of highly efficient perovskite solar cells. Energy Environ Sci 2017;10:710–27.
[2] Saliba M, Correa-Baena JP, Grätzel M, et al. Perovskite solar cells: from the atomic level to film quality and device performance. Angew Chem Int Ed 2018;57:2554–69.
[3] Sum TC, Mathews N. Advancements in perovskite solar cells: photophysics behind the photovoltaics. Energy Environ Sci 2014;7:2518–34.
[4] Kim HS, Lee CR, Im JH, et al. Lead iodide perovskite sensitized all-solid-state submicron thin film mesoscopic solar cell with efficiency exceeding 9%. Sci Rep 2012;2:591.
[5] Michael M, Lee JT, Miyasaka T, et al. Efficient hybrid solar cells based on meso-superstructured organometal halide perovskites. Science 2012;38:643–7.
[6] Stranks SD, Eperon GE, Grancini G, et al. Electron-hole diffusion lengths exceeding 1 micrometer in an organometal trihalide perovskite absorber. Science 2013;342:341–4.
[7] Cho AN, Park NG. Impact of interfacial layers in perovskite solar cells. ChemSusChem 2017;10:3687–704.
[8] Haider M, Zhen C, Wu T, et al. Boosting efficiency and stability of perovskite solar cells with nickel phthalocyanine as a low-cost hole transporting layer material. J Mater Sci Technol 2018;34:1474–80.
[9] Zhang J, Tan CH, Du T, et al. ZnO-PCBM bilayers as electron transport layers in low-temperature processed perovskite solar cells. Sci bull 2018;63:343–8.
[10] Wu W-Q, Chen D, Caruso RA, et al. Recent progress in hybrid perovskite solar cells based on n-type materials. J Mater Chem A 2017;5:10092–109.
[11] Choi J, Song S, Horantner MT, et al. Well-defined nanostructured, single-crystalline TiO_2 electron transport layer for efficient planar perovskite solar cells. ACS Nano 2016;10:6029–36.
[12] Li Y, Zhao Y, Chen Q, et al. Multifunctional fullerene derivative for interface engineering in perovskite solar cells. J Am Chem Soc 2015;137:15540–7.
[13] So F, Kondakov D. Degradation mechanisms in small-molecule and polymer organic light-emitting diodes. Adv Mater 2010;22:3762–77.
[14] Chandiran AK, Yella A, Mayer MT, et al. Sub-nanometer conformal TiO_2 blocking layer for high efficiency solid-state perovskite absorber solar cells. Adv Mater 2014;26:4309–12.
[15] Tavakoli MM, Yadav P, Tavakoli R, et al. Surface engineering of TiO_2 ETL for highly efficient and hysteresis-less planar perovskite solar cell (21.4%) with enhanced open-circuit voltage and stability. Adv Energy Mater 2018;8:1800794.
[16] Tan HR, Jain A, Voznyy X, et al. Efficient and stable solution-processed planar perovskite solar cells via contact passivation. Science 2017;355:722–6.
[17] Tang J, Kemp KW, Hoogland S, et al. Colloidal-quantum-dot photovoltaics using atomic-ligand passivation. Nat Mater 2011;10:765–71.
[18] Anaraki EH, Kermanpur A, Steier L, et al. Highly efficient and stable planar perovskite solar cells by solution-processed tin oxide. Energy Environ Sci 2016;9:3128–34.
[19] Jiang Q, Zhang L, Wang H, et al. Enhanced electron extraction using SnO_2 for high-efficiency planar-structure $HC(NH_2)_2PbI_3$-based perovskite solar cells. Nat Energy 2016;2:16177.
[20] Ke W, Fang G, Liu Q, et al. Low-temperature solution-processed tin oxide as an alternative electron transporting layer for efficient perovskite solar cells. J Am Chem Soc 2015;137:6730–3.
[21] Yang G, Chen C, Yao F, et al. Effective carrier-concentration tuning of SnO_2 quantum dot electron-selective layers for high-performance planar perovskite solar cells. Adv Mater 2018;30:1706023.
[22] Wang P, Jiang Q, Zhao Y, et al. Synergistic improvement of perovskite film quality for efficient solar cells via multiple chloride salt additives. Sci Bull 2018;63:726–31.

Tingting Wu received her Bachelor's degree in Materials Science and Engineering from Shandong University of Science and Technology in 2012. She obtained her Master's degree in Materials Engineering from Institute of Metal Research (IMR), Chinese Academy of Sciences (CAS), in 2015. Currently, she is a Ph.D. candidate at the Institute of Metal Research, University of Science and Technology of China. Her research interests focus on solar cells and photocatalysis under the supervision of Professors Gang Liu and Hui-Ming Cheng.

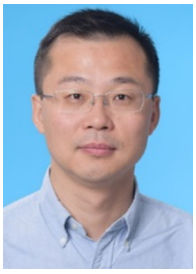

Gang Liu is a Professor and the Deputy Director of Institute of Metal Research, Chinese Academy of Sciences. He received his Bachelor's degree in Materials Physics from Jilin University in 2003 and obtained his Ph.D. degree in Materials Science from Institute of Metal Research in 2009. His main research interests focus on solar conversion materials and devices for renewable energy.